Sintering behaviour of TiO_2-supported model cobalt Fischer-Tropsch catalysts under H_2 reducing conditions and elevated temperature

B.M. Xaba*+, J.P.R. de Villiers*

*+Sasol Group Technology (Pty) Ltd., R & T Division, Sasolburg, 1947, South Africa.

*University of Pretoria, Lynnwood Road, Pretoria, South Africa, 0028, South Africa

KEYWORDS: TiO2, sintering, cobalt, anatase, rutile, P25, crystallite, particle size, GPLE

ABSTRACT: The sintering of model TiO2-supported cobalt catalysts has been studied. The TiO2 supports used were anatase, P25 (85% anatase-15% rutile) and rutile. The catalysts were characterized at each stage of treatment. These treatment stages were calcination, reduction and sintering. It was found that the TiO2 support does not influence the Co3O4 crystallite and particle size as shown by powder x-ray diffraction (XRD) and transmission electron microscopy (TEM) respectively. The reduction of the cobalt catalysts and bare supports was studied by temperature programmed reduction (TPR). It was found that the bare supports were not as inert as expected. The supports showed minor reduction as seen in the H2 consumption. All the cobalt catalysts showed a two-step reduction. Sintering of anatase-supported cobalt was shown to be the most substantial with P25- and rutile-supported showing a lower sintering tendency; P25-supported cobalt being the most stable based on TEM measurements. Sintering kinetics based on the Generalized Power law Expression (GPLE) model, showed that sintering of anatase-supported cobalt is the most rapid with a large sintering rate constant. Sintering of P25-supported cobalt is the lowest, shown by the lowest sintering rate constant. The study has conclusively shown the effect of the catalyst support phase. The study has also shown that the use of high surface area supports is not necessarily the only answer to preventing sintering. The phase of the catalyst support is also important.

INTRODUCTION

Gas-to-liquid (GTL) technology has been shown to provide clean fuels compared to the crude-oil derived counterparts. GTL technology is primarily concerned with the conversion of natural gas into liquid hydrocarbon fuels, through the Fischer-Tropsch synthesis (FTS) process [1]. Major industrial players in GTL and hydrocarbon synthesis technology include Sasol and Shell. Sasol is currently operating a GTL plant in Ras Lafan, Qatar. The plant is a joint venture between Sasol and Qatar Petroleum. The plant named Oryx GTL has a capacity of 34 000 bpd and uses Sasol proprietary Slurry Phase Distillate (Sasol SPD™) technology [2,3].

Typical FTS catalysts are either cobalt- or iron-based depending on the product of interest. These active metals are supported on high surface area oxide supports such as Al_2O_3, SiO_2 and TiO_2 [4,5]. Cobalt and iron-containing catalysts are used in low-temperature FTS to produce high molecular weight hydrocarbons. Iron catalyst is used in high-temperature FTS to produce gasoline and linear low molecular weight olefins. Cobalt is more preferred due to its high per pass FT activity, low oxygenate and CO_2 selectivity compared to iron [1]. Deactivation of cobalt-based catalysts remains a major challenge facing the commercial users of GTL technology as the cobalt metal and noble metal usually used as promoters are expensive [1,6].

Deactivation is expressed as loss of catalytic activity with time on stream. Deactivation mechanisms for cobalt-based catalysts include (i) poisoning by sulphur and nitrogen compounds, (ii) cobalt oxidation, (iii) cobalt-support compound formation, (iv) sintering of cobalt crystallites, (v) surface reconstruction and (vi) carbon deposition. Of all the deactivation mechanisms stated, sintering, carbon formation and surface reconstruction are said to be intrinsic to cobalt and therefore will be present in most cobalt catalyst systems [7,8]

Sintering in this context can be defined as the change in dispersion of the active metal during use or during treatment at high temperatures. Sintering results in loss of catalytic surface area due to crystal growth or loss of support area due to collapse of support [9,10]. There are two generally accepted mechanisms of sintering in supported catalyst systems: Ostwald ripening (OR), and particle migration or coalescence (PMC). Ostwald ripening is defined as the migration of atomic species or molecular species [11]. Coalescence is the migration of whole particles or crystallites until collision with other particles. Coalescence occurs due to weak contact between the particle and the support. This results in the diffusion or migration of the entire particle.

The kinetics of sintering has been studied extensively. Empirical models which describe the sintering behaviour have been developed. These empirical models give kinetic param-

eters such as sintering kinetic constant and activation energy [9,12,13,14]. The Simple Power Law Expression (SPLE) which describes the sintering rate in terms of normalized dispersion and sintering kinetic constant was developed by Ruckenstein & Pulvermacher [12]. In the equation (1), D is the dispersion at time t, D_o is the initial dispersion, k_s is the sintering constant and n is the sintering order. The sintering order n can vary between 2 – 15 for a specific catalyst system at specific temperature. This model has been criticized for this exact reason. This varying of n even for a specific catalyst, makes it difficult to calculate the sintering kinetic constant which is representative of the catalyst system. The calculated values usually do not correlate with experimental data.

$$\frac{-d(D/D_0)}{dt} = k_s \left(\frac{D}{D_0}\right)^n \qquad (1)$$

The SPLE model was later refined by Fuentes et al. [15] to include a term that accounts for the dispersion at infinite time. This term describes the limiting dispersion. The modified model is known as the Generalized Power Law Expression (GPLE) and was described in detail by Bartholomew [16]. In the GPLE equation, D_{eq} is the limiting dispersion and m is the sintering order as shown in equation 2. The GPLE allows for comparison of sintering behaviour of a wide range of catalyst systems. It has been shown that sintering data of various catalyst systems can be fitted well to first- or second-order GPLE where $m = 1$ or $m = 2$ respectively [17].

$$\frac{-d(D/D_0)}{dt} = k_s \left[\left(\frac{D}{D_0} - \frac{D_{eq}}{D_0}\right)\right]^m \qquad (2)$$

Studies have been reported on the sintering of cobalt supported on Al_2O_3, SiO_2 and carbon [2,7,17,18]. Overett et al. [4] studied sintering of a commercial cobalt catalyst supported on Al_2O_3 under realistic FTS process conditions in a 100 barrel/day slurry bubble column reactor (SBCR). The authors used TEM and H_2 chemisorption to deduce that sintering occurred after 3 days on line. It was concluded that sintering accounts for a large percentage of deactivation of the catalyst. Sadeqzadeh et al. [17] studied sintering of cobalt catalyst supported on Al_2O_3 in the presence of water under FTS conditions. They reported that, at the same gas hourly space velocity, sintering proceeds rapidly at higher H_2/CO ratios. The authors also reported that sintering proceeds rapidly in the presence of water at FTS conditions. In a recent paper, Claeys et al. [2] studied the sintering of cobalt supported on Al_2O_3 as a function of process conditions in real time using a novel in situ magnetometer. The authors asserted that CO and high water partial pressure are required for sintering to occur under FTS conditions. They proposed that sintering of cobalt occurs via formation of subcarbonyl species that get transported over the hydroxylated Al_2O_3 support surface.

The effect of water on the sintering of cobalt catalysts was previously reported by Bezemer et al. [19]. The authors observed sintering of cobalt supported on carbon nanofiber in the presence of water under simulated FTS conditions. Sintering was confirmed by TEM, H_2 chemisorption and in situ Mössbauer spectroscopy. The studies of Bezemer et al. and Claeys et al. show that the effect of water on the sintering of cobalt may be the same for Al_2O_3 and carbon supports. Storsæter et al. [20] have previously shown that the effect of water on the activity of Al_2O_3- and SiO_2-supported cobalt catalysts is similar, resulting in rapid deactivation and little recovery of activity after removal water. TiO_2 however was shown to behave differently in terms of deactivation in the presence of water. This support showed no permanent deactivation after water removal compared to Al_2O_3 and SiO_2. This was attributed to the large size of the Co_3O_4 particles supported on the TiO_2 support. The metal-support interaction was also alluded to as a possible reason for the stability of Co/TiO_2 catalyst.

Sintering has been reported for SiO_2-supported cobalt catalysts. In a recent study, Kistarmurthy et al. [18] have studied the sintering of cobalt supported on model planar SiO_2 under model FTS conditions. The authors reported that Ostwald ripening was the dominating sintering mechanism under model FTS conditions in contrast to other reports in literature. The authors concur with the findings of Claeys et al. in which it was deduced that sintering of cobalt occurs via the formation of subcarbonyl species in the presence of CO [18]. A highlight from the work of Kistarmurthy et al. was the use of in situ TEM to study sintering of cobalt particles at identical locations under FTS conditions. The study of particles under realistic reactions conditions has always been a challenge especially in the field of microscopy. The cited literature concurs that the presence of CO and high water partial pressures at FTS conditions are required for sintering to occur. However other parameters can also influence sintering of cobalt catalysts. These include gas environment, temperature, preparation method, pretreatment and support type [17].

TiO_2 was the support of interest in our study. TiO_2 occurs in different crystalline phases which are rutile, anatase and brookite [21,22,23]. The current study follows on the work of Shimura et al. [24] in which they showed the effect of the TiO_2 crystal phase on the activity of TiO_2 –supported cobalt catalysts. The deactivation of cobalt FTS catalysts supported on TiO_2 has recently been reported by Eschemann & de Jong[25]. The authors studied Co/TiO2 FTS catalysts prepared by different synthesis and drying protocols. They reported that all catalysts, irrespective of the preparation protocol, underwent deactivation. The deactivation reported as 20% activity loss, was fully linked to sintering of the active metal. This study conclusively demonstrates the impact of sintering as a deactivation mechanism. It should be noted however, that the authors used only one type of TiO2 support (i.e. P25). Therefore the effect of the TiO2 phase cannot be quantified in their study. The current study aims to leverage the ground work of the cited studies, with the view of establishing the effect of the TiO_2 phase on the sintering behaviour of Co particles.

The TiO_2-supported catalysts in our study were prepared and characterized after calcination and reduction treatment steps. The sintering of TiO_2-supported cobalt crystallites was studied as a function of time and TiO_2 phase under H_2/Ar reducing conditions and at elevated temperature. Sintering

was determined from powder x-ray diffraction (XRD) and high angle annular dark-field-scanning transmission electron microscopy (HAADF-STEM) measurements. Scanning transmission electron microscopy-energy dispersive x-ray spectroscopy (STEM-EDX) was used to ascertain that the particles studied are cobalt particles, through elemental mapping. The average particle size data from TEM was expressed as relative dispersion and was fitted to the GPLE sintering model. The sintering mechanism was then deduced from TEM images by conjecture.

EXPERIMENTAL SECTION

Materials: Three TiO_2 supports were used for the study. These consisted of anatase and rutile TiO_2 phases at different ratios. A BASF TiO_2 which consists of 100% anatase phase was used as the pure anatase support. The Evonik P25 TiO_2 which consists of 85% anatase and 15% rutile phases was used as the mixed-phase support. A rutile support was derived from P25 TiO_2 by calcination in a muffle furnace at 700°C for 8 hours to convert most of the anatase phase into rutile. The resulting material consisted of 98% rutile and 2% anatase phases. Cobalt catalysts were prepared via slurry impregnation of the supports with aqueous solutions of cobalt acetate tetrahydrate. The cobalt loading was kept constant at 10 wt%. The catalysts were calcined in a fluidized bed in air at 300°C for 6 hours. The calcined catalysts were reduced in a mixture of 4% H_2 in argon at a fixed temperature of 450°C, followed by passivation in flowing CO_2.

Sintering studies were performed at 365°C. This temperature is higher than the Hüttig temperature of cobalt (250°C). In this temperature regime, sintering is most likely to occur even in the absence of CO and water. A Carbolite cylindrical furnace was used. The furnace was controlled by a Rex P300 temperature controller. The catalyst powder was placed in a double-walled glass tube which had a porous bottom in the inside. The glass tube allowed gases to flow through the catalyst bed resulting in a fluidized catalyst bed. A gas mixture of 4% H_2 in argon was used for sintering studies. The furnace was heated to 365°C at a rate of 10°C/min. After the sintering hold time was completed, the glass tube was removed from the furnace and the gas flow was switched to CO_2. The CO_2 was allowed to flow through the catalyst bed for 1 hour to passivate the sintered catalyst from re-oxidation. The cooled catalyst powder was sampled for analysis.

Characterization Methods: A Panalytical X'Pert Pro multipurpose diffractometer with a cobalt source (λ = 1.7889 Å) was used for XRD analysis. The instrument was fitted with the X'Celerator detector. The tube voltage was kept at 40 kV and the tube current at 40 mA. A fixed divergance slit was used. Phase identification was performed by X'Pert HighScore Plus software V2.2.1. The relative abundances and crystallite sizes were calculated by the Rietveld refinement method using Topas software V4.2. The fundamental parameter approach was used for profile fitting. Full pattern refinement was performed for crystallite size determination. High temperature XRD reduction was done in an Anton Paar XRK600 cell coupled to a Panalytical X'Pert Pro multipurpose diffractometer with a cobalt source and an X'Celerator detector. The tube voltage was kept at 40 kV and the tube current at 50 mA. A Soller slit of 0.04 rad was used. An fixed divergence slit was used (20). The reduction was done in pure H_2 gas flow. The cell was heated to 380°C at 10°C/min. Scans were collected at intervals of 2 minutes.

An FEI Technai Osiris was used for TEM analysis. The instrument has a field emission gun as an electron source. Bright field (BF) images were acquired on a Gatan CCD camera that was controlled by Gatan Digital Micrograph software. STEM images were captured by a HAADF-STEM detector that was controlled by FEI TIA software. EDX elemental mapping was performed using ChemiSTEM EDX detector system controlled by Bruker Espirit software. The sample was prepared by crushing and mixing with ethanol to form a suspension. The suspension was placed in an ultrasonic bath to disperse the particles into fine particulates. After ultrasonication, a small amount of sample was transferred into a copper TEM grid (SPI Supplies, 300 mesh) using a pipette. The copper grid was placed in a single-tilt TEM specimen holder and transferred into the TEM for analysis. Image J software V1.47u was used for image processing. Crystallite sizes were measured from TEM images after scale calibration and processing.

A Micromeritics ASAP 2420 Surface Area and Porosity analyser was used for Brunauer-Emmett-Teller (BET) surface area and pore size measurements. A sample mass of approximately 0.25 g was weighed into a glass tube. The tube was connected to the degassing port in the instrument. The sample was degassed by heating to 250°C under nitrogen flow for 6 hours. After degassing, the sample tube was weighed after cooling to room temperature. The sample tube was then connected to the analysis port in the instrument. BET surface area and pore sizes were measured at nitrogen relative pressures ranging from 0.08 to 0.98 (p/po). The temperature during analysis was kept at ~77 K (-195°C) by submerging the sample glass tube in liquid nitrogen. Micromeritics ASAP 2420 software V2.04 was used to calculate BET surface area and pore sizes.

A Micromeritics Autochem 2920 TPR instrument was used for temperature programmed reduction (TPR) analysis. A sample mass of approximately 50 mg was weighed into a U-shaped quartz tube, which was then plugged with quartz wool. The sample was dried by heating to 120°C at a rate of 5°C /min under helium gas flow of 50 ml/min. Drying was performed for 10 minutes. The sample was cooled to room temperature.

The cooled sample tube was connected to the instrument and the sample was heated to 900°C at a rate of 10°C /min under a 10% hydrogen/argon mixture flow. The temperature was kept at 900°C for 10 minutes. The hydrogen consumed during the reduction reaction was measured by a thermal conductivity detector (TCD) detector.

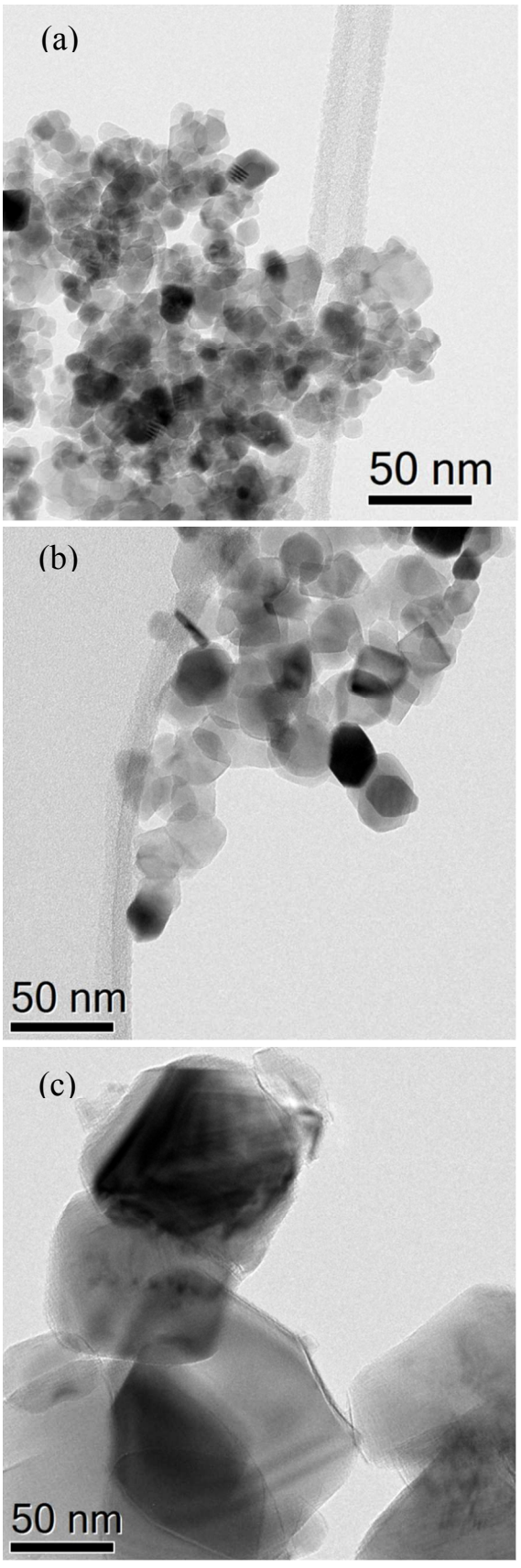

Figure 1: BF-TEM images of TiO2 supports. (a) Anatase, (b) P25, (c) Rutile

RESULTS AND DISCUSSION

Support Characterization: Table 1 lists the XRD results of the bare supports. The results showed that the supports are composed of anatase and rutile phases at different abundances. The results of anatase-support showed that the support is composed of pure anatase. The P25-support was shown to consist of a higher abundance of anatase than rutile. The P25-derived rutile-support was shown to consist predominantly of rutile and minor remnant of anatase at an abundance of 3%.

TEM images of the supports are shown in Figure 1. The particle sizes measured from HAADF images were fitted to lognormal distribution functions to obtain statistical data such as the mean and full width at half-maximum (FWHM). The anatase-support consisted of particles with a size ranging from 6 nm – 22 nm. The mean particle size was calculated as 11.7 nm, with a FWHM of 8.1 nm. The P25-support consisted of two classes of particles. The first class of particles has sizes ranging from 6 nm – 20 nm. These were assumed to be anatase particles. Ohno et al have reported similar sizes for anatase particles in P25 TiO_2 [26]. The second class is that of particles with a size ranging from 20 nm – 50 nm. These can be assumed to be rutile particles [26,27]. The overall mean particle size obtained from the PSD was found to be 22.8 nm with a FWHM of 16.1 nm. The rutile-support had particles with a size ranging from 60 nm – 120 nm. The mean particle size was calculated to be 79.7 nm with a FWHM of 71.1 nm. Overall TEM results were shown to be in agreement with XRD results given in Table 1 in terms of the particle size of TiO_2 particles.

The textural properties of the supports are given in Table 1. The anatase-support was shown to have the highest BET surface area while the rutile-support had the smallest surface area. The surface area can be seen as decreasing with increasing rutile content. It is expected that an increase in this phase will lead to depletion of pore structure and subsequent surface area. The pore size of the supports was also determined as shown in Table 1. The anatase-support had the smallest pore diameter while P25-support has the largest pore diameter. The trend with respect to the pore diameter is P25 > rutile > anatase.

Catalyst Characterization: Table 2 shows the qualitative XRD results of the TiO_2-supported catalysts calcined at 300°C. The results showed the presence of Co_3O_4 spinel, anatase, rutile. The abundance of Co_3O_4 was shown to be similar in the anatase- and P25-supported catalysts. The abundance was lower in the rutile-supported catalyst. The rutile-supported catalyst also showed the presence of $CoTiO_3$ in addition to the other phases. This explains the lower Co_3O_4 abundance. The absence of this phase in the other supported catalysts points to the preferential formation of $CoTiO_3$ in the presence of rutile. This observation was confirmed in other TiO_2-supported catalysts prepared from anatase-, P25- and rutile-supports calcined at different temperatures.

The cobalt oxide crystallite sizes determined by XRD from line broadening using volume-based column height function L_{Vol} are given in Table 3. The results showed relatively larger cobalt crystallites in anatase-supported catalyst, while similar sizes were observed in P25- and rutile-supported catalysts. It is proposed that the presence of rutile leads to a stability of Co_3O_4 particles formed during calcination, an effect absent in the anatase -based catalyst. The Co_3O_4 crystallites formed in the anatase support could possibly undergo slight growth during calcination resulting in the observed increase in crystallite size.

TEM results of the calcined catalysts given in Figure 2 revealed the size of the Co_3O_4 particles and their spatial distribution over the supports. STEM-EDX mapping of the catalysts confirmed the composition and spatial distribution of the cobalt oxide particles. This is especially useful in the case where some particles of the TiO_2 support have the same size as the Co_3O_4 particles.

Therefore in the case where the particle size of the support and metal oxide are similar, EDX mapping becomes important to differentiate between particles. The separate EDX maps showing the distribution of Co and Ti are shown in Figure 2. Images of the EDX maps superimposed on the HAADF-STEM images are also given.

Table 1: Physical and Textural properties of the TiO2-supports used in the study

Support	**% Phase Composition**		**BET surface area (m2/g)**	**Average Pore size (nm)**
	Anatase (3σ error)	Rutile (3σ error)		
Anatase	100 (0.3)	0 (0.3)	109	9.8
P25	84 (0.6)	16 (0.6)	52	26.9
Rutile	3 (0.3)	97 (0.3)	8	22.8

Table 2. Phase composition of TiO_2-supported catalysts

Catalyst	**% Phase Composition**			
	Anatase (3σ error)	Rutile (3σ error)	Co3O4 (3σ error)	CoTiO3 (3σ error)
Co/Anatase	87 (0.2)	1 (0.2)	12 (0.2)	0
Co/P25	73 (0.2)	14 (0.1)	13 (0.1)	0
Co/Rutile	0 (0.4)	85 (0.4)	9 (0.2)	6 (0.1)

Table 3. Crystallite size (XRD) and particle size (TEM) of Co_3O_4 and Co^0 in the TiO_2-supported catalysts

Catalyst	**Co3O4 size (nm)**		**Co^o size (nm)**	
	XRD	TEM (size range)	XRD	TEM (size range)
Co/Anatase	33	17 (5 – 40)	36	21 (5 – 40)
Co/P25	29	33 (5 – 70)	28	53 (20 – 120)
Co/Rutile	29	19 (5 – 40)	19	20 (3 – 40)

The images of the anatase-supported catalyst showed Co3O4 particles with a size ranging from 5 nm – 40 nm. The mean particle size was smallest in this support. The images of the P25-supported catalyst showed Co3O4 particles with a size ranging from 5 nm – 70 nm. The mean particle size was found to be the largest in this support. The Co3O4 particles in the rutile-supported catalyst were shown to range from 5 nm – 40 nm.

The Co3O4 particle sizes from TEM can be correlated to the pore sizes of the support given in Table 1. It was shown that P25 had the largest pore size, while anatase support had the smallest pore size. The correlative trend may indicate pore size effects in the catalysts.

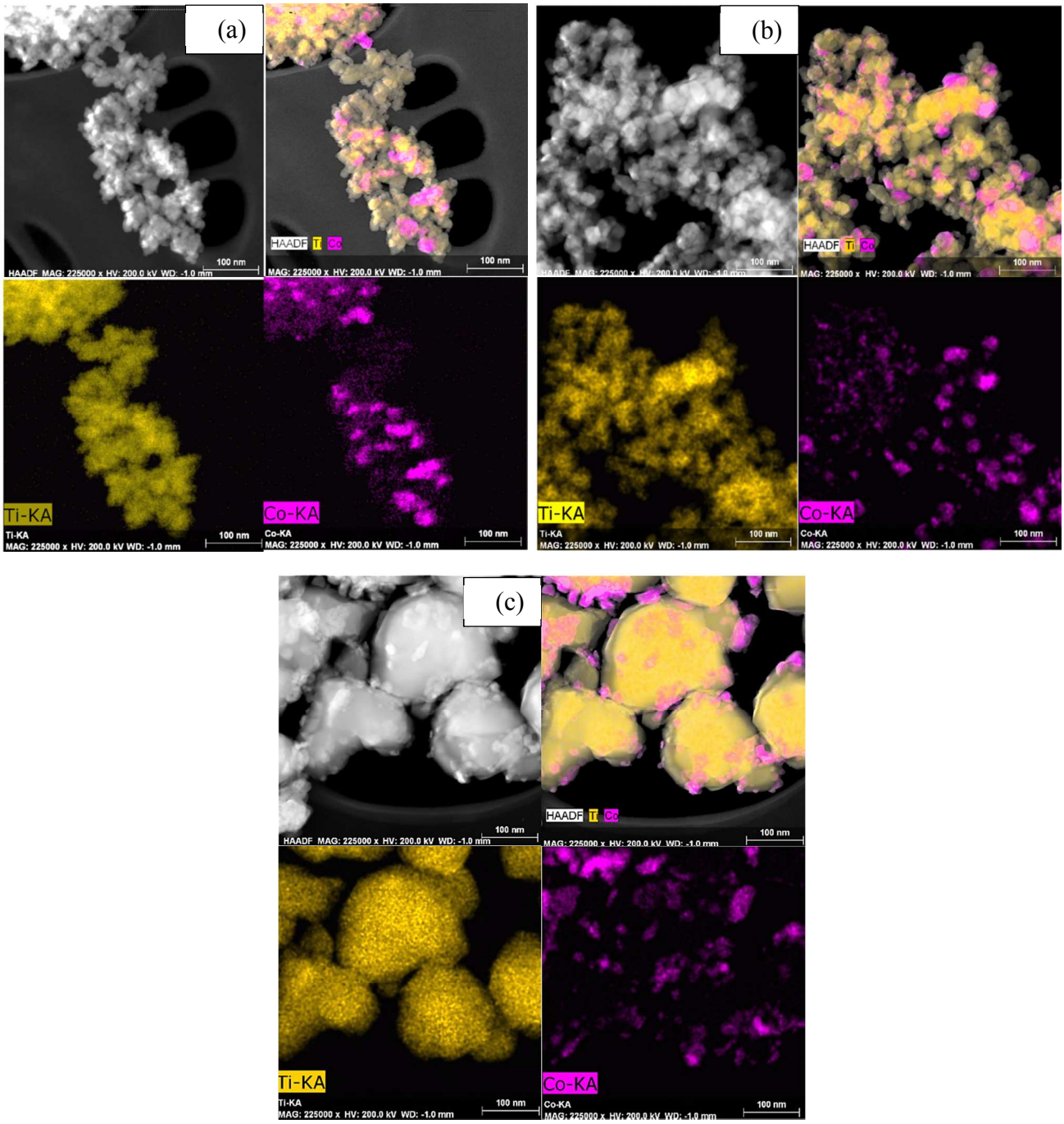

Figure 2: HAADF-STEM-EDX mapping images of calcined TiO_2-supported cobalt catalysts (a) Co/Anatase, (b) Co/P25 and (c) Co/Rutile showing the distribution of cobalt oxide particles across the different supports.

Catalyst Reduction: Temperature programmed reduction was conducted to study the reduction behaviour of the TiO_2-supported catalysts. The TPR profiles of the bare supports are given in. Figure 3. The results showed that the TiO_2 supports were not as inert as initially expected. The results showed an uptake of H_2 in all supports, indicating some extent of reduction. The profiles of P25 and rutile supports show a distinct peak at ~315^{o}C. This peak is absent in anatase support. However, all the supports show a broad peak with a maximum between 500^{o}C - 600^{o}C.

The observation of support reduction is in agreement with the work of Xiong et al, [28]. These authors reported that TiO2 reacted with hydrogen at a temperature below 300^{o}C. As the temperature increases to above 300^{o}C, electrons become transferred from the H atoms to O atoms in the lattice of TiO2. As the O atom interacts with H atoms to form H2O, oxygen vacancies are created. As the temperature increases

up to 450°C, the interaction of TiO2 with hydrogen intensifies with the evolution of Ti3+. These Ti3+ entities are formed due to the electron transfer from oxygen vacancies to Ti4+ ions. As the temperature increases to above 560°C, more energy was supplied resulting in more electrons being transferred from the oxygen vacancies to the Ti4+. The possibility of forming surface defects in the TiO2 supports in our study exists. This process can occur through H2 spillover during reduction of cobalt crystallites [29].

The TPR profiles of the TiO2-supported catalysts given in Figure 3 show a two-step reduction of cobalt oxide to metallic cobalt. The peak at ~310oC can be assigned to the reduction of Co3O4 to CoO. The peaks between 450°C - 500°C can be assigned to the reduction of CoO to metallic cobalt. The profiles of the different TiO2 supported catalysts are different indicating different interactions of the metal oxide and supports. There are also minor peaks at low temperatures in the anatase-supported catalyst. These peaks are likely resulting from the reduction of residual material from the precursor. The first major reduction peak position is similar in all the catalysts. However, the second reduction peak appears at higher temperatures for anatase- and rutile-supported catalysts. The peak is at a lower temperature in P25-supported catalyst. The higher reduction temperature implies that the second reduction to metallic cobalt is difficult in both anatase and rutile supports. This can be linked to the possible formation of surface defects such as oxygen vacancies and Ti intestitials as a result of support reduction. It is known that defects can be induced on the surface of TiO2 phases with annealing under reducing conditions [21]. This phenomenon can have implications on the sintering behavior of cobalt crystallites.

The XRD volume-based crystallite sizes of metallic cobalt obtained from line broadening are given in Table 3. The crystallite size of anatase-supported cobalt was shown to be 36 nm. The crystallite sizes of P25- and rutile-supported cobalt were shown to be 28 nm and 19 nm respectively. The results are consistent with the trend observed in Co_3O_4 crystallite size across the supports. In this case, the anatase-support showed a relatively larger crystallite size compared to P25 and rutile supports.

HAADF-STEM images combined with EDX maps of the reduced & passivated catalysts are given Figure 4. The images show the distribution and size of cobalt particles. The anatase-supported cobalt size was found to range between 5 – 40 nm. The P25-supported cobalt size was found to range between 20 – 120 nm. The rutile-supported cobalt size was shown to range between 3 – 40 nm. The trend is consistent with that observed in Co_3O_4 particle size across the supports. In this case, the Co on the P25-support shows a relatively larger particle size compared to the other supports.

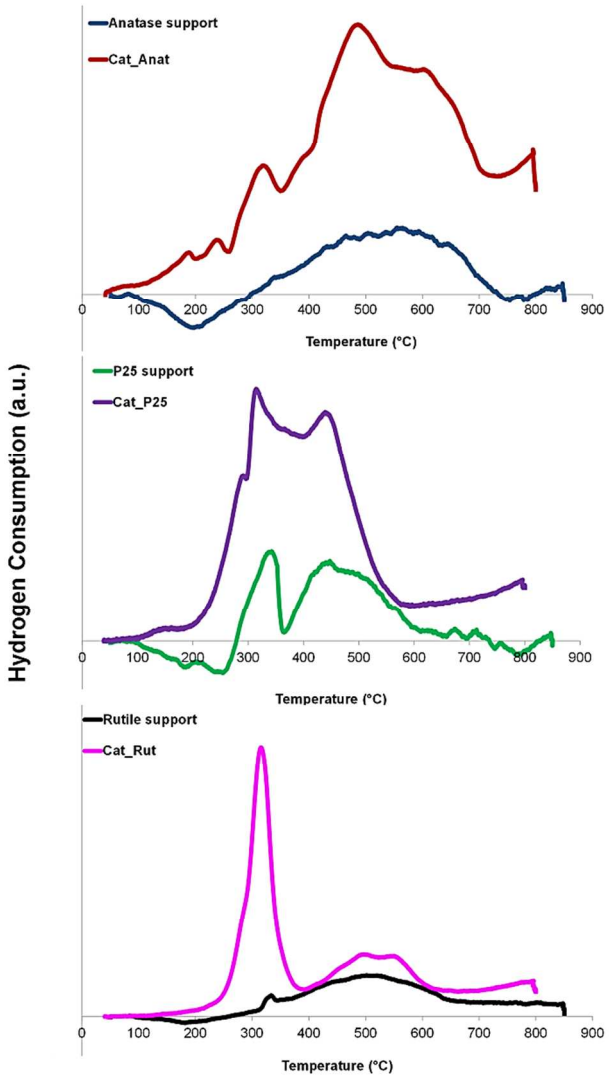

Figure 3: Temperature programmed reduction (TPR) of bare TiO2 supports and TiO2-supported cobalt catalysts.

It is also interesting to note the similar particle sizes in anatase and rutile supports from a TEM point of view, despite the contrasting phase compositions seen in XRD analysis.

This is in contrast to the findings of Shimura et al.[24]. The authors observed large cobalt particles in a TiO2 support consisting of 100% anatase phase from TEM, compared to a support consisting 85% anatase and 15% rutile phases. They proposed that there is a relatively strong interaction between cobalt and rutile which suppresses growth of cobalt particles by aggregation. This strong interaction is absent in the anatase support hence the growth of particles. From our study, the proposal of Shimura et al. [24] actually agrees with the XRD results which showed larger crystallites on the anatase support compared to the rutile support.

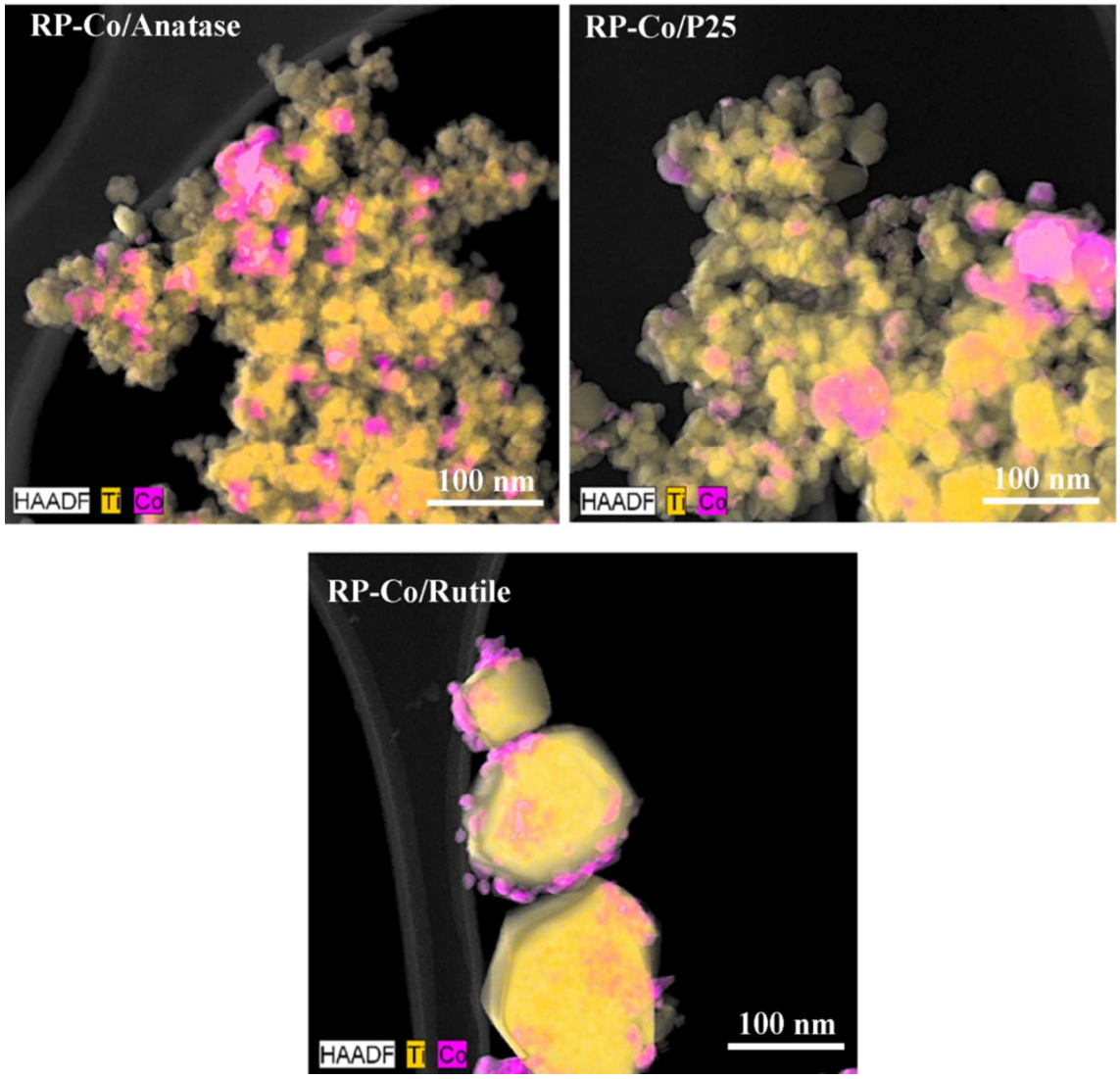

Figure 4: HAADF-STEM-EDX mapping images of reduced and passivated TiO_2-supported cobalt catalysts showing the distribution of metallic cobalt particles across the different supports.

Sintering Studies: Sintering was studied by XRD and TEM. The cobalt crystallite and particle size data is given in Table S1 in the Supporting Information. From XRD data the anatase-supported cobalt crystallite size shows an increase from 31 nm (at 4 hours) up to 55 nm (at 48 hours). The P25-supported crystallite size increases from 26 nm (at 4 hours) up to 35 nm (at 48 hours). The rutile-supported crystallite size shows a mild increase from 25 nm (at 4 hours) to 28 nm (at 48 hours). The trend in sintering from XRD measurements is: anatase > P25 > rutile.

The cobalt particle sizes from TEM are given in Table S2 in the Supporting Information. The PSDs are given in Figure 5. The particle size of anatase-supported cobalt increased from 30 nm (at 4 hours) up to 88 nm (at 48 hours). This amounts to ~65% growth in size. The P25-supported cobalt particle size showed a mild increase from 51 nm (at 4 hours) up to 65 nm (at 48 hours). This amounts to 22% growth. The rutile-supported cobalt particle size showed an increase from 17 nm (at 4 hours) up to 36 nm (at 48 hours), indicating a 53% growth. The trend in sintering from TEM measurements is: anatase > rutile > P25.

XRD and TEM measurements show differences which can be linked to the inherent differences in their measurement principles. XRD measures the crystallite size as the size of the smallest coherently scattering domain of the material [30]. On the other hand, TEM measures the particle as a 2D projection. The contrast results from differences in the atomic number of the element, the so-called z-contrast, compared to the difference in phase composition and diffraction that is encountered in XRD. In addition, XRD gives a volume-average crystallite across the whole sample, while TEM gives a number-based count of individual particles as seen on a TEM micrograph [31]. Nonetheless it is clear from both XRD and TEM that severe sintering is observed in anatase supported catalysts.

In light of the apparent differences in crystallite and particle size data, further examination of the differences in sintering behavior of the TiO_2-supported catalysts was based on TEM particle sizes. This is because TEM particle sizes can be expressed particle size distributions (PSD) which are useful in studying sintering. Furthermore, TEM allows for the direct viewing of sintered particles which is useful for deducing sintering mechanisms.

The kinetics of sintering was examined to compare the sintering behavior of the TiO_2-supported catalysts. The particle size data was expressed as relative dispersion and was fitted to the GPLE model [16]. The first-order GPLE gave the best fit to our data. The sintering rate constants and estimated limiting dispersion are given in Table 4. The results show that anatase-supported particles undergo rapid sintering as shown in Figure 6 and characterized by a large sintering rate constant. The rutile-supported catalyst shows the second largest sintering rate constant. The lowest sintering rate constant is that of P25-supported catalyst indicating the lowest propensity for sintering. It is interesting to note that the sintering rate constant of P25-supported catalyst is ten times smaller than that of rutile-supported catalyst, and orders of magnitude smaller than that of anatase-supported catalyst. This highlights the propensity of sintering and the effect of the support. This is in an important finding since it highlights that high surface area supports are not necessarily effective at preventing sintering of supported catalysts. Other support properties have to be taken into consideration.

Table 4: Sintering rate constants and limiting dispersion of TiO_2-supported catalysts

Catalyst	Do	Deq	GPLE rate constant (h-1)
Anatase	4.72	1.50	0.25
P25	1.88	0.09	0.01
Rutile	5.14	2.75	0.06

Factors that may explain the difference in sintering of the TiO_2-supported catalysts are phase of the support, metal-support interaction, defects on the surface of the TiO_2 phase and pore size of the support.

It is know that the support can interact strongly with the crystallites in different ways. When the catalyst system is exposed to a reduction treatment, depending on whether the crystallite or support is mobile, different metal-support interaction scenarios can result [32]. It has been shown that when the crystallites are mobile, and when cohesive forces between particles are greater that the adhesive forces between the crystallite and support, agglomeration occurs. In this case, the support does not retain the crystallites strongly and they are able to agglomerate. However in the case where the adhesive forces between the support and crystallite are greater than the cohesive forces between crystallites, the crystallites become attached strongly over the support forming the so-called "pill-box" interaction where the crystallite wets the support [16,32]. This strong interaction might inhibit growth of these crystallites, especially by coalescence mechanism. This might be the case for rutile-supported crystallites in our study. Chen et al. [33] observed a similar effect in TiO_2-supported nickel catalysts. In their study, rutile-supported nickel crystallites were observed to be small and better dispersed compared to anatase-supported nickel crystallites. They concluded that the difference in crystallite size and dispersion was due to different metal-support interaction.

Defects on the surface of the TiO_2 phase may also be of important in the interaction and sintering of cobalt crystallites. It is known that defects such as oxygen vacancies and Ti interstitials exist in the surface and bulk of TiO_2 phases, especially after reduction treatment. It has been shown that defects are likely to form on the surface of rutile rather than in the bulk since this phase is more stable. In the case of anatase, the defects are likely to form in the bulk rather than on the surface since this phase has the lowest surface free energy. It has been shown that metals preferentially form bonds on the defect sites on the surface of TiO_2 [21]. In this case, the defect site acts as an anchor for the metal onto the TiO_2 support.

The sintering behaviour of cobalt crystallites in the TiO2-supports may be correlated to the effect of defect sites. In the case of the reduced rutile support, the presence of surface defects may provide anchorage sites thereby inhibiting growth by coalescence or migration. In the case of the Anatase support, these defects are likely to be found in the bulk, therefore cobalt crystallites on the surface may not bound so strongly and subsequently agglomerate or coalesce. An interesting case arises with P25 support. It is known that this support consists of anatase, rutile and amorphous material in intimate contact [34]. In some cases it has been shown that small rutile crystallites are interwoven with anatase crystallites and in some cases rutile forms a surface layer onto anatase crystallites [35].

It is thought that this intimate contact of the phases will enhance their interaction and further stabilise particles supported on the support as evidenced by the lowest sintering rate constant of P25-supported crystallites.

The sintering mechanism of supported cobalt particles under our current experimental conditions was determined from TEM images by conjecture. This part of the study was not as rigorously approached as that of Kistamurthy et al. [18]. In this part we merely highlight the possible mechanisms under our experimental conditions. Analysis of particles from TEM images leads us to believe that both OR and PMC occur in all the TiO2 supports used in our study. The question of which is the dominating mechanism is not clear. The evidence of PMC is shown in Figure 7. In these images,

the presence of conjoined particles is shown. In some cases the particles form a "strip" or "ribbon-like" structures resulting from particle migration or coalescence. In the case of OR, it cannot be ruled out since it is possible that gaseous species can evolve at the relatively high temperature used in our study. Similar results have been reported by Hansen et al. [36]. The authors reported that both OR and PMC occur at different stages in supported catalysts.

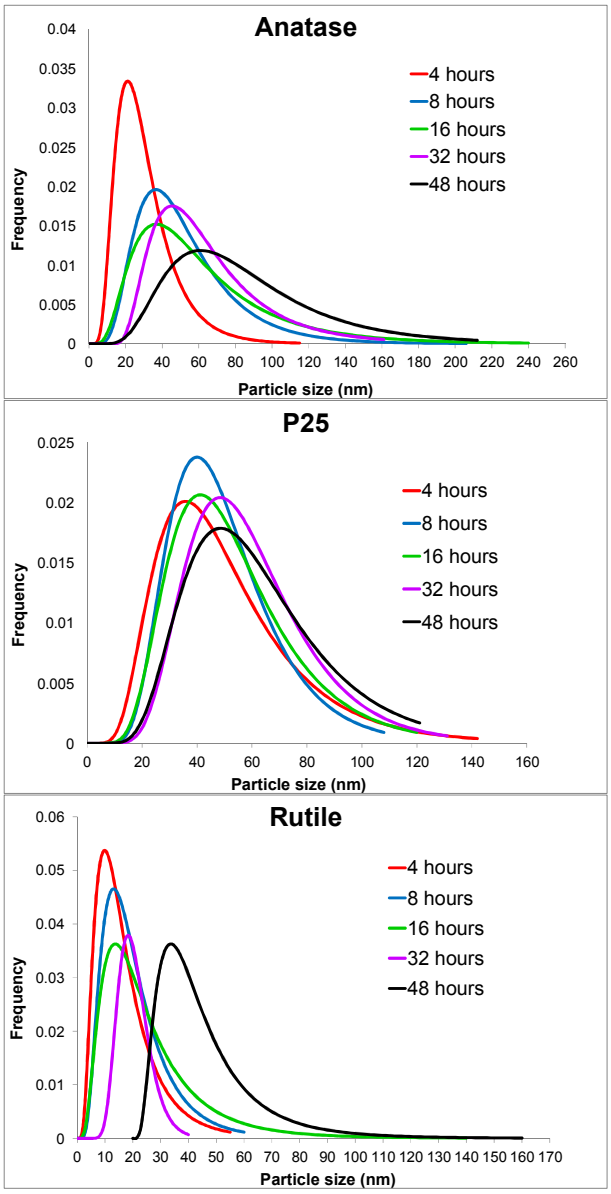

Figure 5: Particle size distribution curves fitted onto lognormal distribution functions showing the effect time on the crystallite size of TiO_2-supported catalysts.

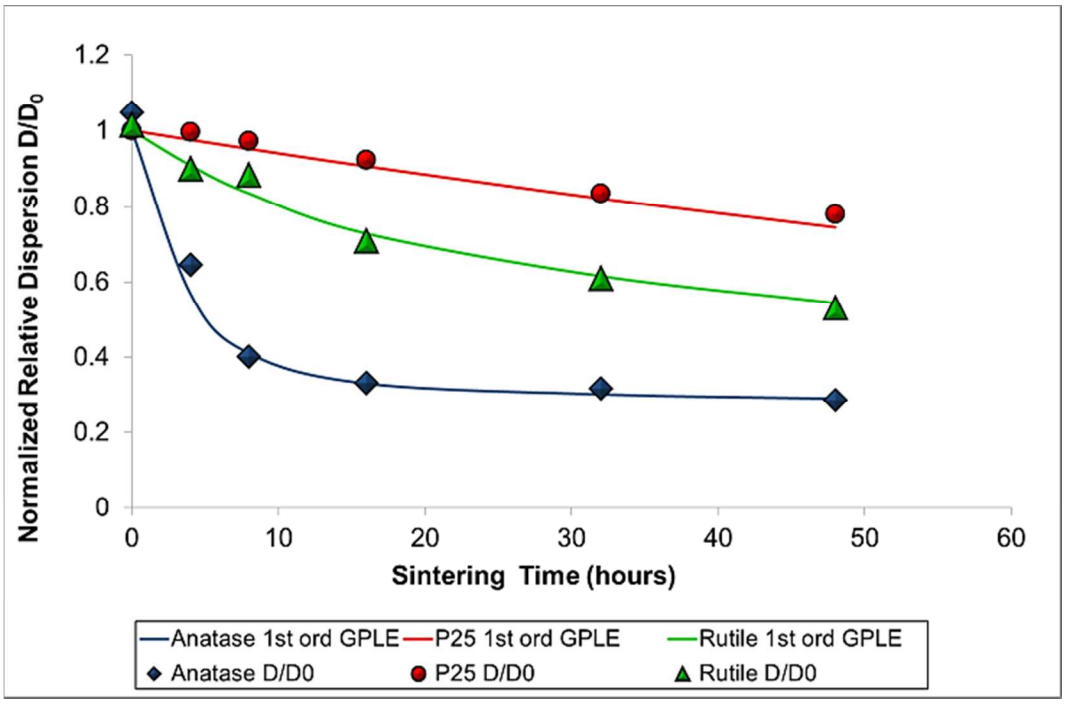

Figure 6: Plots of normalized relative dispersion against sintering time for TiO_2 supported catalysts fitted onto 1st order GPLE

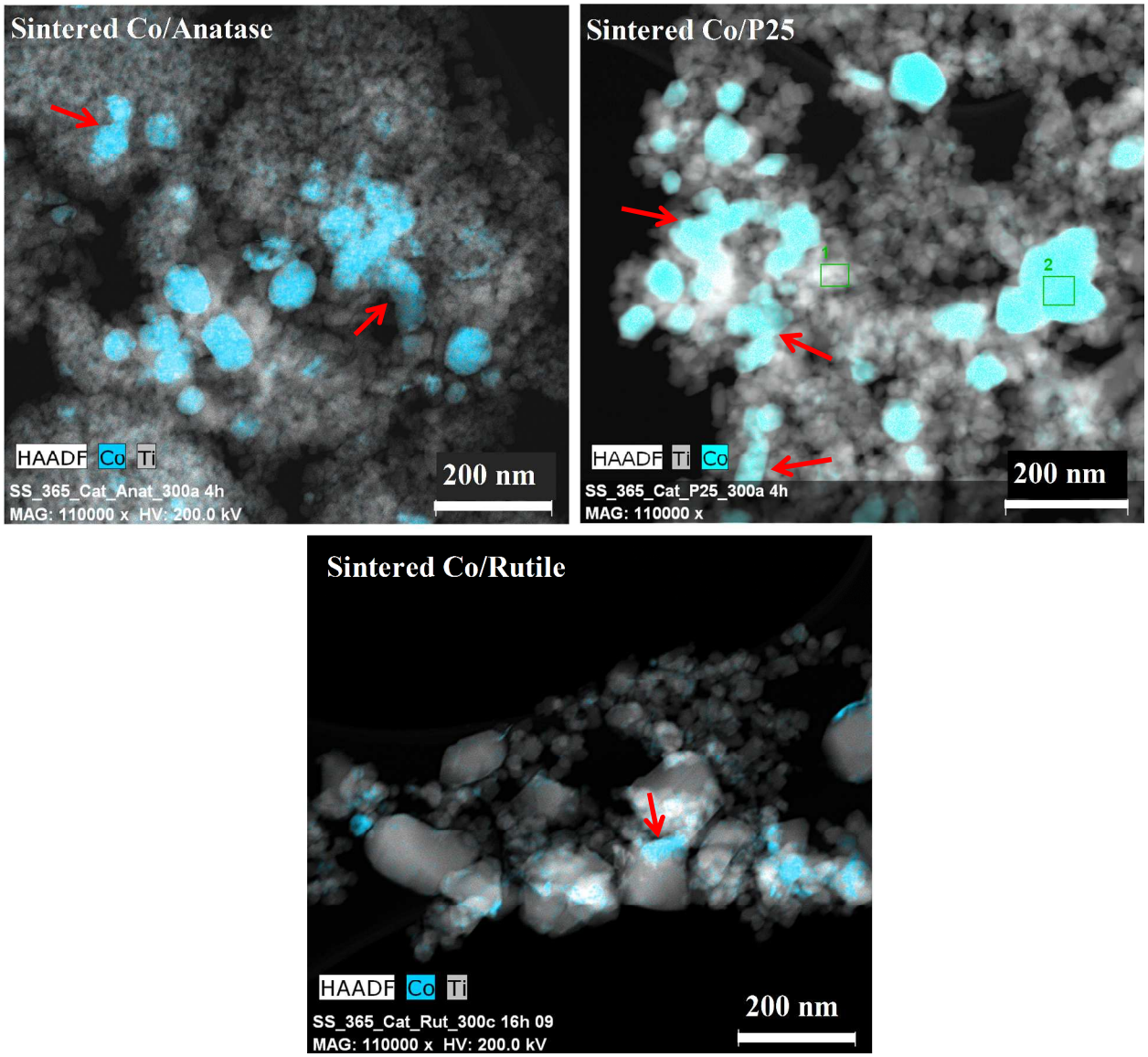

Figure 7: HAADF-STEM images with EDX mapping superimposed showing the evidence of PMC occurring in the sintered TiO_2 supported catalysts indicated by red arrows.

The atmosphere and temperature in which sintering is studied has been shown to be of importance. The studies of Kistarmurthy et al. [18] and Claeys et al. [2] showed that CO is required for sintering of cobalt particles to take place at the operating temperature of FTS (210°C – 230°C). Bezemer et al. [19] showed that the presence of high water partial pressure also induces sintering of cobalt particles at the FTS operating temperatures (210°C – 230°C). We report herein, that even in the absence of CO and water vapour sintering of cobalt particles can occur. However, elevated temperatures are required for this to take place. Therefore, the sintering observed in our study is temperature-induced. It is know that the Tamman and Hüttig temperatures of cobalt are 604°C and 253°C respectively [2,18]. The current study was conducted at a temperature higher than the Hüttig temperature, but smaller that the Tamman temperature. It is expected that in this temperature range sintering is imminent even in the absence of CO and water vapour. The current study is therefore of importance for reduction stages of FTS where H2 reduction is performed at elevated temperatures.

CONCLUSIONS

The sintering of model unpromoted TiO_2-supported cobalt catalysts has been studied. The properties of the bare TiO_2 supports were initially established. The supports consisted of different TiO_2 phases. The supports also had different surface areas and pore sizes.

It was shown that the TiO_2 support influences the particle size of Co_3O_4 as measured by TEM. The reduction of Co_3O_4 to metallic cobalt was shown to be similar in all the supports. An important finding from TPR analysis was that the TiO_2 supports are not as inert as initially envisaged. It was shown that the bare supports undergo mild reduction upon expo-

sure to H_2. It is expected that should this occur in supported catalysts, it may influence the metal-support interaction. The TiO_2 was shown to influence the metallic cobalt particle size.

Sintering of anatase-supported cobalt was shown to be the most substantial. P25 and rutile showed a lower sintering tendency, P25-supported cobalt being the most stable. Sintering kinetics based on the GPLE model showed that sintering of anatase-supported cobalt is the most rapid with a large sintering rate constant. Sintering of P25-supported cobalt is the lowest, shown by the lowest sintering rate constant. Sintering of rutile-supported cobalt is lower than that of anatase-supported cobalt, but ten times higher than that of P25-supported cobalt. The study conclusively showed the effect of the TiO_2 support. It has also been shown that the use of high surface area supports is not necessarily effective in preventing sintering of supported particles. Metal-support interaction has to be taken into account as well.

SUPPORTING INFORMATION

The Supporting Information is available for further reference. The following information is available:

EDX spectra of TiO_2 supports showing elemental composition; XRD diffractograms showing phase composition of the TiO_2 supports; particle size distribution data and plots.

AUTHOR INFORMATION

Corresponding Author

+ E-mail: Bongani.xaba@sasol.com

ACKNOWLEDGMENTS

The financial support from Sasol Group Technology, National Research Foundation and the University of Pretoria is gratefully acknowledged.

REFERENCES

(1) Moodley, D.J.; van de Loosdrecht, J.; Saib, A.M.; Overett, M.J.; Datye, A.K.; Niemantsverdriet, J.W. Carbon deposition as a deactivation mechanism of cobalt-based Fischer-Tropsch synthesis catalysts under realistic conditions. *Appl. Catal. A: Gen*. **2009**, 354, 103.

(2) Claeys, M.; Dry, M.E.; van Steen, E.; van Berge, P.J.; Booysens, S.; Crous, R.; van Helden, P.; Labuschagne, J.; Moodley, D.J.; Saib, A.M. Impact of Process Conditions on the Sintering Behavior an Alumina-Supported Cobalt Fischer-Tropsch Catalyst Studied with an in Situ Magnetometer. *ACS Catal.* **2015**, 5, 841.

(3) Leckel, D. Diesel Production from Fischer-Tropsch: The Past, the Present, and New Concepts. *Energy & Fuels*. **2009**, 23, 2342.

(4) Overett, M.J.; Breedt, B.; du Plessis, E.; Erasmus, W.; van de Loosdrecht, J. Sintering as a deactivation mechanism for cobalt supported on alumina Fischer-Tropsch catalyst. *Am. Chem. Soc. Div. Pet. Chem.* **2008**, 53, 127.

(5) Saib, A.M.; Borgna, A.; van de Loosdrecht, J.; van der Berge, P.J.; Niemantsverdriet, J.W. Preparation and characterization of spherical Co/SiO2 model catalysts with well-defined nano-sized cobalt crystallites and comparison of their stability against oxidation with water. *J. Catal.* **2006**, 239, 326.

(6) Tsakoumis, N.E.; Rønning, M.; Borg, Ø.; Rytter, E.; Holmen, A. Deactivation of cobalt based Fischer-Tropsch catalysts. *Catal. Today*. **2010**, 154, 162.

(7) Sadeqzadeh, M.; Chambrey, S.; Hong, J.; Fongarland, P.; Luck, F.; Currulla-Ferre, D.; Schweich, D.; Bousquet, J.; Khodakov, A.Y. Effect of different reaction conditions on the deactivation of alumina-supported cobalt Fischer-Tropsch catalysts in a milli-fixed-bed reactor: Experiments and modelling. *Ind. Eng. Chem. Res.* **2014**, 53, 6915.

(8) Saib, A.M.; Moodley, D.J.; Ciobica, I.M.; Hauman, M.M.; Sigwebela, B.H.; Westrate, C.J.; Niemantsverdriet, J.W.; van de Loosdrecht, J. Fundamental understanding of deactivation and regeneration of cobalt Fischer-Tropsch synthesis catalysts *Catal. Today*. **2010**, 154, 271.

(9) Flynn, P.C.; Wanke, S.E. Experimental studies of sintering of supported platinum catalysts. *J. Catal.* **1975**, 34, 395.

(10) Bartholomew, C.H. Mechanisms of catalyst deactivation. *Appl. Catal. A.* **2001**, 212, 35.

(11) Simonsen, S.B.; Chorkendorff, I.; Dahl, S.; Skogludh, M.; Sehested, J.; Helveg, S. Ostwald ripening in a Pt/SiO2 model catalyst studied by in-situ TEM. *J. Catal.* **2011**, 281, 147.

(12) Ruckenstein, E.; Pulvamacher, B. Growth kinetics and size distributions of supported metal crystallites. *J. Catal.* **1973**, 29, 224.

(13) Fiedorow, R.M.J.; Wanke, S.E. The sintering of supported metal catalysts I. Redispersion of supported platinum in oxygen. *J. Catal.* **1976**, 43, 43.

(14) Wynblatt, P.; Gjostein, N.A. Supported metal crystallites. *Prog. Solid. State. Chem.* **1975**, 9, 21.

(15) Fuentes, G.A. Catalyst deactivation and steady-state activity: A generalized power-law equation model. *Appl. Catal.* **1985**, 15, 33.

(16) Bartholomew, C.H. Sintering kinetics of supported metals: New perspectives from a unifying GPLE treatment. *Appl. Catal.* **1993**, 107, 6.

(17) Sadeqzadeh, M.; Hong, J.; Fongarland, P.; Luck, F.; Currulla-Ferre, D.; Schweich, D.; Bousquet, D.; Khodakov, A.Y. Mechanistic modelling of cobalt-based catalyst sintering in a fixed bed reactor under different conditions of Fischer-Tropsch synthesis. *Ind. Eng. Chem. Res.* **2012**, 51, 11955.

(18) Kistamurthy, D.; Saib, A.M.; Moodley, D.J.; Niemantsverdriet, J.W.; Westrate, C.J. Ostwald ripening on a planar Co/SiO_2 catalyst exposed to model Fischer-Tropsch synthesis conditions. *J. Catal.* **2015**, 328, 123.

(19) Bezemer, G.L.; Remans, T.J.; van Bavel, A.P.; Dugulan, A.I. Direct evidence of water-assisted sintering of cobalt on carbon nanofiber catalysis during simulated Fischer-Tropsch conditions revealed with in-situ Mössbauer spectroscopy. *J. Am. Chem. Soc.* **2010**, 132, 8540.

(20) Storsæter, S.; Borg, Ø.; Blekkan, E.A.; Holmen, A. Characterization of alumina-, silica-, and titania-supported cobalt Fischer-Tropsch catalysts. *J. Catal.* **2005**, 236, 143.

(21) Diebold, U. Structure and properties of TiO_2 surfaces: A brief review. *Appl. Phys. A.* **2002**, A76, 1.
(22) Li, G.; Li, L.; Zheng, J. Understanding the defect chemistry of oxide nanoparticles for creating new functionalities: A critical review. *Sci. China. Chem.* **2011**, 54, 876.
(23) Hanaor, D.A.H.; Sorrell, C.C. Review of the anatase to rutile phase transformation. *J. Mater. Sci.* **2011**, 46, 856.
(24) Shimura, K.; Miyazawa, T.; Hanaoka, T.; Hirata, S. Fischer-Tropsch synthesis over TiO_2-supported cobalt catalysts: Effect of TiO_2 crystal phase and metal ion loading. *Appl. Catal. A: Gen.* **2013**, 460-461, 8-14.
(25) Eschemann, T.O.; de Jong, K.P. Deactivation behavior of Co/TiO_2 catalysts during Fischer-Tropsch synthesis. *ACS Catalysis*, **2015**, 5, 3181
(26) Ohno, T.; Sarukawa, K.; Tokieda, K. Matsumura, M. Morphology of a TiO_2 photocatalyst (Degussa P25) consisting of anatase and rutile crystalline phase. *J. Catal.* **2001**, 203, 83.
(27) Datye, A.K.; Riegel, G.; Bolton, J.R.; Huang, M.; Prairie, M.R. Microstructural characterization of a fumed Titanium Dioxide photocatalyst. *J. Solid State Chem.* **1995**, 115, 236.
(28) Xiong, L.B.; Li, J.L.; Yang, B.; Yu, Y. Ti^{3+} in the surface of titanium dioxide: Generation, properties and photocatalytic application. *J. Nanomater.* **2012**, 2.
(29) Bernal, S.; Calvinio, J.J.; Cauqui, M.A.; Gatica, J.M.; López Cartes, C.; Pérez Omil, J.A.; Pintando, J.M. Some contributions of electron microscopy to the characterization of the strong metal-support interaction effect. *Catal. Today.* **2003**, 77, 385.
(30) Akbari, B.; Pirhadi Tavandashti, M.; Zandrahimi, M. Particle size characterization of nanoparticles: A practical approach. *Iranian J. Mater. Sci. & Eng.* **2011**, 8, 50.
(31) Ozkaya, D. Particle size analysis of supported platinum catalysts by TEM. *Platinum Metals Rev.* **2008**, 52, 61.
(32) Deutschmann, O.; Knozinger, H.; Kochloefl, K.; Turek, T. Heterogeneous catalysis and Solid catalysts. *Ullmann's Encycl. Ind. Chem.* **2009**, 1- 110.
(33) Chen, R.; Du, Y.; Xing, W.; Xu, N. The effect of titania structure on Ni/TiO2 catalysts for p-nitrophenol hydrogenation. *Chin. J. Chem. Eng.* **2006**, 14, 667.
(34) Hurum, D. C.; Agrios, A. G.; Gray, K. A. Explaining the enhanced photocatalytic activity of Degussa P25 mixed-phase TiO_2 using EPR. *J. Phys. Chem. B.* **2003**, 107, 4546.
(35) Bickley, R. I.; Gonzalez-Carreno, T.; Lees, J. S.; Palmisano, L.; Tilley, R. J. D. A structural investigation of titanium dioxide photocatalysts. *J. Solid State Chem.* **1991**, 92, 180.
(36) Hansen, T. W.; DelaRiva, A. T.; Challa, S. R.; Datye, A. K. Sintering of catalytic nanoparticles: Particle Migration or Ostwald ripening? *Acc. Chem. Res.* **2013**, 46, 1725.

Graphical abstract